HHS Public Access

Author manuscript

Biol Psychiatry. Author manuscript; available in PMC 2024 February 02.

Published in final edited form as:

Biol Psychiatry. 2024 February 01; 95(3): 266–274. doi:10.1016/j.biopsych.2023.07.013.

Manipulating ΔFOSB in D1-type Medium Spiny Neurons of the nucleus accumbens reshapes whole brain functional connectivity

Marion Sourty[1,2,§], **Md Taufiq Nasseef**[3,4,§], **Cédric Champagnol-Di Liberti**[1], **Mary Mondino**[2], **Vincent Noblet**[2], **Eric M. Parise**[5], **Tamara Markovic**[5], **Caleb J. Browne**[5], **Emmanuel Darcq**[1,3], **Eric J Nestler**[5,*], **Brigitte L. Kieffer**[1,3,*]

[1.]INSERM U1114, University of Strasbourg, Strasbourg 67084, France

[2.]iCube, University of Strasbourg-CNRS, Strasbourg France

[3.]Douglas Research Center, Department of Psychiatry, McGill University, Montréal, Quebec H4H 1R3, Canada

[4.]Department of Mathematics, College of Science and Humanity Studies, Prince Sattam Bin Abdul Aziz University, Saudi Arabia

[5.]Nash Family Department of Neuroscience, Friedman Brain Institute, Icahn School of Medicine at Mount Sinai, New York, NY USA 10029

Abstract

BACKGROUND.—The transcription factor, ΔFOSB, acting in the nucleus accumbens (NAc), has been shown to control transcriptional and behavioral responses to opioids and other drugs of abuse. However, circuit-level consequences of ΔFOSB induction on the rest of the brain—required for its regulation of complex behavior—remain unknown.

METHODS.—We used an epigenetic approach in mice to suppress or activate the endogenous *Fosb* gene, and therefore decrease or increase, respectively, levels of ΔFOSB selectively in D1-type medium spiny neurons of the NAc, and tested whether these modifications affect the organization of functional connectivity (FC) in the brain. We acquired fMRI images at rest and in response to a morphine challenge, and analyzed both stationary and dynamic FC patterns.

RESULTS.—The two manipulations markedly and differently modified brain wide communication. ΔFOSB down- and up-regulation had overlapping effects on prefrontal- and retrosplenial cortex-centered networks, but also generated specific FC signatures for epithalamus (habenula) and dopaminergic/serotonergic centers, respectively. Analysis of dynamic FC patterns showed that increasing ΔFOSB essentially altered responsivity to morphine, and uncovered

Co-corresponding authors: **Brigitte L. Kieffer**, INSERM U1114 University of Strasbourg, CRBS 1 rue Eugène Boeckel, CS60026 67084 Strasbourg Cedex France, brigitte.kieffer@unistra.fr, **Eric J. Nestler**, Nash Family Department of Neuroscience and Friedman Brain Institute, Icahn School of Medicine at Mount Sinai, 1 Gustave L. Levy Place, Box 1065, New York, NY 10029; eric.nestler@mssm.edu.

[§]First co-authors

[*]Last co-authors

striking modifications of epithalamus and amygdala roles in brain communication, particularly upon ΔFOSB down-regulation.

CONCLUSIONS.—These novel findings illustrate how it is possible to link activity of a transcription factor within a single cell type of an identified brain region to consequent changes in circuit function brain-wide by use of fMRI, and pave the way for fundamental advances in bridging the gap between transcriptional and brain connectivity mechanisms underlying opioid addiction.

Keywords

Fosb gene expression; bi-directional epigenetic manipulation; mouse fMRI; brain connectivity; prefrontal cortex; habenula

INTRODUCTION

Opioid use disorder (OUD) represents one of today's greatest public health threats, yet our understanding of the underlying neurobiology and our ability to treat the syndrome remain limited. Additionally, there remain today no established biological approaches to track addiction-related brain changes in OUD patients to assist with diagnosis and to track treatment during abstinence, with a current sole reliance on behavioral signs and symptoms of the disorder.

Prior research has implicated transcriptional regulation in mediating the long-term effects of opioids on the brain's reward circuitry (1, 2), a major component of which is the nucleus accumbens (3). The transcription factor, ΔFOSB, has been shown to be a major driver of such transcriptional pathology in the NAc: viral-mediated or genetic overexpression of ΔFOSB in NAc neurons increases the rewarding responses to opioids, while blockade of ΔFOSB function has the opposite effects (4). Chronic exposure to opioids induces ΔFOSB in both major subtypes of NAc medium spiny projection neurons (MSNs) (5), which are classified as D1-type or D2-type based on the dopamine receptor that they predominantly express. Similar patterns of ΔFOSB induction are seen in response to contingent vs. non-contingent opioid administration (5). The ability of ΔFOSB to promote opioid reward is related to its actions in D1 MSNs, however circuit consequences of ΔFOSB induction in NAc D1 MSNs, through which the transcription factor drives its influence on opioid reward, have not yet been characterized.

To address this question, we conducted functional magnetic resonance imaging (fMRI) in mice (6–10). We used a suite of locus-specific epigenome editing tools that either activate the *Fosb* gene and increase expression of endogenous ΔFOSB or suppress the *Fosb* gene and decrease ΔFOSB expression levels (11, 12). We targeted these epigenome editing tools —expressed with viral vectors—to D1 MSNs by use of mice that express Cre recombinase selectively in this cell type. We then subjected the mice to fMRI at baseline and in response to an acute dose of morphine, and studied functional connectivity (FC). Our findings identify novel regions of the brain's reward circuitry that are affected upon manipulation of ΔFOSB expression levels in D1 MSNs, and reveal ΔFOSB-dependent FC signatures.

METHODS AND MATERIALS

See Supplementary Information for detailed Methods and Materials

Animals

D1-Cre bacterial artificial chromosome transgenic male mice (http://www.gensat.org/cre.jsp) were bred at the Icahn School of Medicine at Mount Sinai, according to the Institutional Animal Care and Use Committee guidelines at Mount Sinai and the Canadian Council of Animal Care (more details in Suppl Information).

Viral treatment

Fosb-targeting zinc finger proteins (ZFPs) were manufactured by the CompoZr ZFN Operations Group at Sigma-Aldrich Biotechnology and cloning steps performed as previously described (11). Stereotaxic surgeries targeting the NAc were performed as reported (13). Validation of expression site and cellular specificity of *FosB*-targeting viruses was performed using FISH (Suppl Information and Suppl Fig. S1).

MRI experiments

MRI data acquisition was achieved using a 7T small animal scanner. Animals were sedated using a combination of isoflurane and dexmedetomidine (14), and their physiological parameters carefully monitored. Images were obtained using Spin Echo EPI pulse sequence, see details in Suppl Information.

MRI Data analysis

Preprocessing steps are described in Suppl Information. Brain parcellation was based on the Allen Brain Mouse Atlas, and included either 120 seeds or regions of interests (ROIs) covering the entire brain (Suppl Fig. S3, Suppl Table S1), or 23 selected ROIs (Suppl Fig. S4 and Suppl Table S2). Postprocessing steps included FC mapping at baseline (1–9min) and post-morphine (18–26min), as well as analysis of the dynamics of the FC patterns over the entire duration of the fMRI (see Suppl Information).

RESULTS

Experimental Design

Male D1-Cre mice were injected in the NAc with either control (CTL, n=12), ΔFOSB-downregulating (G9a, n=13) or ΔFOSB-upregulating (P65, n=13) AAV vectors. AAV-ZFP-G9a expresses a synthetic zinc finger protein (ZFP) that selectively targets the *Fosb* gene promoter fused to G9a, a repressive histone methyltransferase, while AAV-ZFP-P65 expresses the same ZFP fused to P65, which promotes histone acetylation (11, 12). These epigenome-editing tools have been shown to effectively decrease (G9a) or increase (P65) endogenous ΔFOSB expression in a cell-type-specific manner in the NAc. We again validated this regulation in the present experiment: the control (CTL) AAV vector expressing a non-targeting ZFP (ASSB) fused to P65 had no effect on ΔFOSB expression, while the G9a and P65 viruses decreased and increased ΔFOSB levels in the mouse NAc, respectively (Suppl Fig. S2). After 5 weeks of recovery and habituation to the MRI animal facility,

mice were lightly anesthetized and placed in the 7T Bruker scanner (see Methods). Image acquisition was performed for 30 min, which included 10 min at rest followed by an intrascanner s.c. injection of a single morphine dose (10 mg/kg) while image acquisition was continued for another 20 min (Suppl Fig. S5). The latter morphine challenge was included in the experimental design with the goal of revealing FC alterations that may otherwise not be detectable at baseline.

Both G9a and P65 mice show altered functional connectivity patterns brain wide

After image preprocessing (see Methods), several animals whose images showed motion artifacts and excessive deformation at normalization with the Allen Brain Atlas were excluded from the analyses (Suppl Information). For the remaining animals (CTL n=9, G9a n=9 and P65 n=7), examination of anatomical images (Suppl Fig. S6) confirmed that the NAc was accurately targeted. Of note, examination of functional images showed deformation essentially at the level of the anterior cingulate area (ACA).

We first analyzed stationary network characteristics, considering 1–9 min (baseline or BSL) and 18–26 min (under morphine or MOR) time periods. Time series were extracted for 120 ROIs covering the entire brain (7140 seed pairs, see Suppl Fig. S3, Suppl Table S1), and CC values were computed for each seed pair and animal and averaged per group (see Methods), leading to 6 datasets: CTL mice at baseline (CTL-BSL) or under morphine (CTL-MOR), G9a at baseline (G9a-BSL) or under morphine (G9a-MOR) and P65 at baseline (P65-BSL) or under morphine (P65-MOR). To examine similarities of connectivity patterns across the six groups, we performed hierarchical clustering of CC values from each group (see Methods and Fig. 1A). The dendrogram showed a first separation between CTL and G9a/P65 groups (1), demonstrating that the two genetic manipulations (up- and down-regulation of ΔFOSB) markedly altered brain connectivity. The next separation was for P65-BSL and P65-MOR groups (2), showing that P65 mice were most different from CTL and G9a mice. Finally, BSL and MOR groups formed closest clusters in all cases (CTL, G9a or P65 treatment), which was expected as datasets for BSL and MOR animals were extracted from the same individuals. Notably, however, P65-BSL and P65-MOR were most distinct, suggesting that morphine had a stronger effect on P65 mice (3).

To better understand the nature of brain modifications that underlie these observations, we simplified datasets by considering a smaller number of ROIs, i.e., ROIs with functional relevance to ΔFOSB biology, addiction and depression networks, and also brain areas expressing the mu opioid receptor and responding to morphine. This selection includes 23 brain areas (Suppl Fig. S4), which span forebrain to hindbrain and have variable sizes (from 119 voxels for the dorsal raphe nucleus [DR], to 8020 voxels for the caudate putamen [CP]) (Suppl Table S2). Hierarchical clustering was performed as above, and showed a pattern highly similar to the 120-seed analysis (Fig. 1B): again, CTL groups were most different from G9a and P65 groups (1) and P65 groups separated next (2). As well, P65-BSL and P65-MOR patterns were most different among BSL/MOR clusters. Because conclusions from the 120 and 23 seed-based analyses were similar, we pursued further analyses using the 23 selected seeds.

We next used a sliding window approach and two graph theory metrics to examine dynamic network features indicating how connectivity changed over time for each of the 23 seeds and for each group (see Methods). The two metrics were strength (how one region is connected to the whole network) and centrality (how one region influences the network), respectively (see Methods) and values were computed for the 23 seeds along time for each group and for each time window. For strength (Fig 1C), statistical analysis (t-test, $p<0.05$) identified several time windows at which G9a and P65 values significantly differ from CTL values, confirming that the two epigenetic manipulations reshape brain communication. The analysis of dynamic FC properties also showed further differences between G9a and P65 treatments. Thus, values from G9a mice significantly differed from CTL mice both before and after morphine injection, indicating detectable connectivity modifications whether morphine was present or not. For P65 mice, however, strength showed significant differences mainly in the post-morphine injection period, suggesting that morphine exposure unmasked connectivity alterations in this group. These observations are recapitulated by quantifying the number of time windows with significant difference from the CTL group (Suppl Table S3 and Fig 1C, right panel). For centrality (Fig. 1D), similar observations were made despite the fact this metric is a different measure of FC.

In conclusion these data demonstrate that G9a and P65 treatments in D1 MSNs of the NAc broadly modify brain communication, and suggest that down- and up-regulation of the same transcription factor (ΔFOSB) produce distinct effects, including differential sensitivity to morphine.

G9a and P65 mice differently modify functional connectivity of the brain

Using the 23-seed approach, a total of 253 connections were available, but not all connections showed G9a or P65 effects, or showed sensitivity to morphine. We performed 7 comparisons for each connection, testing either the ΔFOSB manipulation effect (comparison of CTL/G9a or CTL/P65 at BSL and under MOR; two-sample t-test), or the morphine effect (comparison of BSL/MOR, for CTL, G9a and P65 groups; paired t-tests) (Suppl Table S4). We then focused our subsequent analyses on connections that showed significance ($p<0.05$) in any of the t-test comparisons, in order to reduce dimensionality of the data set (90 seed pairs, see Methods and Suppl Table S4).

We next determined the direction of connectivity changes for G9a (Fig. 2A) and P65 (Fig. 2B) mice. The analysis was performed at baseline and under morphine. For G9a mice, we found 31 and 15 seed pairs with decreased (negative values in Fig. 2A) and increased (positive values in Fig. 2A) FC, respectively, indicating that a larger number of connections showed reduced correlated activities. The epithalamus (EPI)-caudate putamen (CP) pair showed the lowest p value (BSL condition, see Suppl Table S4). Contrasting with the G9a data, the P65 treatment led to a higher number of connections having increased FC (31 vs 16 seed pairs), indicating that brain communication was enhanced for a higher number of seed pairs in this group. For P65 mice, periaqueductal gray (PAG)/pontine reticular nucleus (PRN) and PAG/DR showed the lowest p values (MOR condition). This analysis further supports the notion that down- or up-regulation of ΔFOSB in NAc D1 MSNs produces distinct effects on brain communication.

G9a and P65 mice show both common and distinct network signatures

Next, we developed a new approach that would allow the simultaneous analysis of FC for all 23 opioid/ΔFOSB-related seeds of interest. To identify groups of seed pairs that may show correlated activity in the brain (pairs with similar FC patterns across individuals), we clustered CC values of the 90 pairs of interest for all individual animals, whichever treatment or group (see Methods). The resulting dendrogram (Fig. 3A, left) revealed 6 major clusters reflecting networks operating in the brain under our experimental conditions. These clusters, also visualized on circular plots (Fig. 3A, right), include 7 to 20 connections, with typically one or two seeds most highly connected within the network. In cluster 1, EPI (which includes the habenula at the cross-road of forebrain and mid/hindbrain) and SUB (subiculum) were the most connected seeds (7 connections each). Cluster 2 was the smallest, with ACA most connected, but will not be further considered as this region was highly prone to deformations. Cluster 3 was the largest, and most connections in this cluster were linked to the prefrontal cortex (infralimbic [ILA], and prelimbic [PL] areas, 7 connections). Clusters 4 and 5 showed NAc (ACB) as the most connected seed (4 and 5 connections, respectively). In addition, cluster 5 showed high connectivity for the DR (4 connections), representing a cluster including dopamine and serotonin centers. Cluster 6 showed highest connectivity for the retrosplenial cortex (RSP, 5 connections), considered the core center of the Default Mode Network (DMN) (7, 15).

We next determined the effects of ΔFOSB manipulations on FC of these clusters. We compared data from G9a and P65 mice with data from CTL mice at baseline and found two clusters (3 and 6) modified both by G9a and P65 treatments (Suppl Fig. S7). Clusters 3 and 6 therefore represent a general ΔFOSB signature on brain communication whose core centers are (i) the prefrontal cortex (ILA-PL) and its connections with the insular area (AI), the NAc, the globus pallidus (Gpe-Gpi) the basomedial-basolateral amygdala (BLA-BMA), and several hypothalamic nuclei, and (ii) the RSP in interaction with the forebrain (ILA-PL) and EPI, as well as mid/hindbrain (DR, PAG, ventral tegmental area (VTA) and the pontine reticular nucleus [PRN]) (see Fig. 3B).

This analysis also identified specific clusters uniquely modified by one or the other ΔFOSB manipulation. G9a mice differed from CTL for cluster 1 (Suppl Fig. S7) characterized by EPI and SUB, both connecting with the AI, the striatum (NAc, CP) and hindbrain regions (PAG, parabrachial nucleus or PB), and also connecting together (Fig. 3C). P65 mice showed a specific modification of cluster 5 (Suppl Fig. S7), a signature centered on NAc and DR, their interconnection and their connectivity with hippocampus (dentate gyrus [DG], CA subfields), hypothalamus (lateral hypothalamus [LHA], hypothalamus lateral zone [LZ]) and the hindbrain (PB, midbrain reticular nucleus [MRN]) (Fig. 3D).

In these comparisons, it was interesting to note that morphine modified only cluster 4 in CTL mice (Suppl Fig. S8), indicating that a main target of the opioid drug is a NAc-centered cluster consistent with known morphine effects on this major reward processing center. Cluster 4 was also modified by morphine in P65 mice, but not G9a mice (not shown), (Suppl Fig. S8), perhaps reflecting the higher sensitivity of P65 mice to the drug.

G9a mice show striking modification of EPI and amygdala roles within brain functional connectivity

Pursuing the dynamic analysis (Fig 1B), we next identified seeds whose role within brain networks changed upon the epigenetic manipulations for the longest duration. To do so, we quantified the % time where strength and centrality values differed from CTLs along the acquisition, including baseline and morphine conditions, and seeds were ranked accordingly (Suppl Table S3). Individual traces of seeds showing the highest % time are shown in Fig. 4.

For G9a mice (Fig. 4A), strength was most modified for the EPI seed (20.00%, BSL; 16.67%, MOR), indicating that the level of EPI connectivity with the rest of the brain was most altered. Observation of the trace shows both lower and higher strength compared to CTL at baseline, and lower strength under MOR conditions. Medial and central amygdala (MEA-CEA) came next (14.76%, MOR, strength lower than CTL). Centrality also was impaired in G9a mice, in a variable manner for the entire amygdala (BLA-BMA 18.13%, BSL; MEA-CEA 15.63%, BSL; MEA-CEA 33.53%, MOR), the lateral part of the hypothalamus (LHA, 17.50% MOR) and a brainstem nucleus (PRN 15.74%, MOR). The centrality results indicate that G9a impairs the influence of these regions over network activities, an effect particularly strong for the amygdala.

P65 mice show strongest modifications of PRN, BLA/BMA and EPI centralities in response to morphine

For P65 mice (Fig. 4B and Suppl Table S3), strength values were less modified over time. Interesting, however, strength of the NAc (Fig. 4B, top) was strongly enhanced for a short period of time (6–8 min post-injection). This transient effect could not be detected in the stationary analysis, and also was not observed in the neighboring CP seed.

In contrast, centrality was strongly modified for the PRN (20%), BLA-BMA (16.76%) and EPI (15.74%), but only under MOR conditions, confirming that the morphine challenge unmasked network reorganization triggered by P65, as was observed for all 23 seeds (Fig. 1B). Notably, centrality modifications induced by down- and up-regulation of ΔFOSB seemed to oppose each other for amygdala (mostly below CTL for G9a mice and above CTL for BLA/BMA in P65 mice).

DISCUSSION

Prior research has established an important role for ΔFOSB in opioid and other addiction syndromes (1, 16). Opioids and all other drugs of abuse induce ΔFOSB in D1 MSNs of the NAc in rodents (1, 5) and in humans examined postmortem (see (16)). ΔFOSB induction in D1 MSNs in vivo contributes to the transcriptional reorganization that occurs in NAc in response to drug exposure and promotes rewarding responses to opioid and other drugs of abuse (1, 4, 16). Such induction also alters synaptic properties of these neurons recorded *ex vivo* in brain slices (17). However, the missing link in these analyses is how ΔFOSB induction in D1 MSNs and its effects on synaptic plasticity alter the functioning of the brain's larger reward circuitry to ultimately exert effects on complex behavior. The present study represents a key first step in providing this information.

Here we bidirectionally controlled the activity of the endogenous *Fosb* gene, to produce increase or decrease in ΔFOSB levels in D1 MSNs that closely match the magnitude of changes observed i*n vivo* in rodents and humans, and studied the consequences on brain-wide circuit function by use of fMRI. These epigenetic editing tools (11, 12) avoid possible confounds associated with traditional overexpression and knockout approaches (18). Our results establish that manipulation of a single gene (the transcription factor ΔFOSB in this case) within one cell type (D1 MSNs) of a single brain region (NAc) is sufficient to modify whole brain communication as detectable by fMRI in a mouse (Fig 1–3).

Some of our data show a parallel between the bi-directional nature of epigenetic modifications and their consequences on whole brain activity, as we found two examples where down- vs. up-regulation of ΔFOSB expression exert opposite effects on brain connectivity. First, a higher number of seed pairs showed weaker FC in G9a mice, while an opposing effect was observed for P65 mice (Fig. 2). Second, we found reduced vs. increased centrality for amygdalar areas for G9a and P65 mice (Fig. 4), suggesting opposing modifications of amygdala importance within brain networks. Conversely, there was an example where the two manipulations produced a similar effect, i. e. alterations of clusters 3 and 6 (Fig. 3B), centered on (i) cortical areas that exert an essential role on top-down controls (ILA-PL) and influence decision-making processes (19, 20) and (ii) the RSP characterizing the brain at rest and considered a landmark of healthy brain functioning (21) (7). The latter observation suggests that functioning of these particular circuits require an optimal level of ΔFOSB activity, such that pathological deviations in either direction result in shared aspects of circuit dysfunction. One example of such mechanisms could operate via the VTA, which is part of clusters 3 and 6. NAc D1 MSNs innervate both dopaminergic and non-dopaminergic VTA neurons that in turn innervate NAc MSNs. The D1 MSN nerve terminals located in VTA are opioid sensitive, which could potentially explain similar responses to opposite D1 manipulations during morphine administration (22).

The influence of ΔFOSB manipulations on brain responses to morphine were most apparent upon induction by AAV-ZFP-P65. Thus, while ΔFOSB down-regulation (G9a mice) modified functional connectivity whether morphine was present or not, ΔFOSB up-regulation induced modifications detectable essentially under the morphine challenge (Fig. 1B and Fig. 4). Moreover, the stationary analysis showed a strong morphine effect on the NAc-centered cluster (cluster 4), in both CTL and P65 (Suppl Fig S7) but not G9a mice (not shown), and the dynamic analysis revealed a transient but clearly detectable morphine effect on NAc strength in P65 mice (Fig 4B), which was not seen in G9a mice (not shown). Prior work has shown that chronic morphine exposure increases ΔFOSB levels (4) and, further, that ΔFOSB induction in D1 MSNs primes an animal for greater behavioral responses to an opioid or other drugs of abuse (1, 16). The present result showing increased sensitivity of brain networks to morphine upon ΔFOSB induction is in line with the notion that a prior chronic exposure to morphine alters animal responses to subsequent drug exposure, and provides a network hypothesis underlying this phenomenon. Future studies will incorporate behavioral measures with fMRI data in order to directly correlate connectivity signatures of ΔFOSB up-/down-regulation with morphine responses, addiction-related behaviors or emotional dysfunction, which we reported earlier (1, 4, 5, 16). It will also be interesting to examine the influence of chronic opioid exposure on brain FC and how these measures

are affected by preventing ΔFOSB induction with AAV-ZFP-G9a. Likewise, it would be interesting in future investigations to compare the effect of ΔFOSB on brain responses to morphine to those of other drugs of abuse, in particular, stimulants such as cocaine for which ΔFOSB was shown important in the process of addiction. Finally, while we focused here on D1 MSNs, further work is needed to understand the effect of ΔFOSB induction in D2 MSNs. This is of particular interest since opioids, uniquely among drugs of abuse, induce ΔFOSB in both D1 and D2 MSNs (5).

FC of the EPI showed remarkable alterations in G9a mice throughout this study. This seed includes the habenula, a small conserved and increasingly studied brain region regulating information flow across the forebrain and midbrain (23–25). The habenula is sensitive to opioids (26–28) and also considered a key target area to understand and treat addiction and mood disorders (29–34). In G9a mice, the stationary analysis shows a highly significant increase of EPI-CP connectivity at baseline (Fig 2), as well as a specific alteration of an EPI-centered network (network 1, Fig 3C), connecting to the striatum (ACB and CP). Also, the dynamic analysis highlights EPI strength as the most durable alteration (Fig 4A). Together, these results suggest that ΔFOSB down-regulation in D1 MSNs has strongest impact on habenula-associated networks, which has potential consequences on reward and mood processing. Of note, P65 mice also show alteration of EPI centrality post-morphine (Fig. 4B), and the fact that EPI FC is modified by the two ΔFOSB manipulations in the NAc may result from the reported direct connectivity between these two brain areas (35).

FC of the amygdala is dependent on ΔFOSB levels. The amygdala is extensively studied for its roles in fear learning, stress responses and anxiety (for ex (3, 36–38)). Although nothing was detected in the stationary analyses, the dynamic analysis revealed that the most durable modification occurs in BLA-BMA and MEA-CEA for G9a, and come in second for MEA-CEA in P65 mice (Supp Table S3 and Fig 4). These modifications were observed for centrality, but not strength, indicating a modification in the way amygdala activity influences other brain regions upon both up- and down-regulation of ΔFOSB levels in D1 MSNs of the NAc. This finding also highlights the importance of developing dynamic analytic methods in mouse fMRI approaches.

While ΔFOSB action in NAc D1 MSNs is best studied in the context of drug addiction, it has also been shown to play an important role in controlling responses to chronic stress. Induction of ΔFOSB in this cell type enhances resilience in mouse models, whereas humans diagnosed with Major Depressive Disorder show lower levels of ΔFOSB expression at baseline (3, 12, 39). It would therefore be interesting to study stress-related endpoints on further characterization of ΔFOSB's regulation of the brain limbic circuitry by fMRI. Finally, a limitation of the present study is its focus on male mice, and it will be important in the future to conduct similar studies in females (40).

In conclusion, this study illustrates a critical challenge in neuroscience today, namely, to understand how cell-autonomous processes influence brain circuit function to control complex behavior. The present analytical pipeline can now be used to link other key signaling molecules in D1 MSNs, or any other cell type of interest, to downstream changes in brain circuit function.

Supplementary Material

Refer to Web version on PubMed Central for supplementary material.

ACKNOWLEDGMENTS AND DISCLOSURES

This work was supported by the National Institutes of Health (P50DA005010 and R01048796 [to BLK] and P01DA047233 and R01DA007359 [to EJN]), the Canada Fund for Innovation and the Canada Research Chairs [to ED and BLK], We thank the staff of the animal facility of the Neurophenotyping Center of the Douglas Mental Health University Institute (Montréal, Canada), and Jai Puneet Singh for his help in data analysis. The authors would also like to acknowledge the High-Performance Computing Center of the University of Strasbourg for supporting this work by providing scientific support and access to computing resources. Part of the computing resources were funded by the Equipex Equip@Meso project (Programme Investissements d'Avenir) and the CPER Alsacalcul/Big Data.Finally, we thank Laura Harsan for careful reading of the manuscript.

BLK and EJN designed the experiments and provided resources for it. EMP, TM, and CJB generated and validated the viral vectors. TN and ED performed the fMRI experiments. MS and MM preprocessed the data. MS, VN and CC performed the post-processing analyses. BLK and EJN wrote the manuscript. All authors read and approved the submitted version.

The authors report no biomedical financial interests or potential conflicts of interest.

REFERENCES

1. Robison AJ, Nestler EJ (2011): Transcriptional and epigenetic mechanisms of addiction. Nat Rev Neurosci. 12:623–637. [PubMed: 21989194]
2. Browne CJ, Godino A, Salery M, Nestler EJ (2020): Epigenetic Mechanisms of Opioid Addiction. Biol Psychiatry. 87:22–33. [PubMed: 31477236]
3. Koob GF, Volkow ND (2016): Neurobiology of addiction: a neurocircuitry analysis. Lancet Psychiatry. 3:760–773. [PubMed: 27475769]
4. Zachariou V, Bolanos CA, Selley DE, Theobald D, Cassidy MP, Kelz MB, et al. (2006): An essential role for DeltaFosB in the nucleus accumbens in morphine action. Nat Neurosci. 9:205–211. [PubMed: 16415864]
5. Lobo MK, Zaman S, Damez-Werno DM, Koo JW, Bagot RC, DiNieri JA, et al. (2013): DeltaFosB induction in striatal medium spiny neuron subtypes in response to chronic pharmacological, emotional, and optogenetic stimuli. J Neurosci. 33:18381–18395. [PubMed: 24259563]
6. Mechling AE, Arefin T, Lee HL, Bienert T, Reisert M, Ben Hamida S, et al. (2016): Deletion of the mu opioid receptor gene in mice reshapes the reward-aversion connectome. Proc Natl Acad Sci U S A. 113:11603–11608. [PubMed: 27671662]
7. Arefin TM, Mechling AE, Meirsman AC, Bienert T, Hubner NS, Lee HL, et al. (2017): Remodeling of Sensorimotor Brain Connectivity in Gpr88-Deficient Mice. Brain Connect. 7:526–540. [PubMed: 28882062]
8. Ben Hamida S, Mendonca-Netto S, Arefin TM, Nasseef MT, Boulos LJ, McNicholas M, et al. (2018): Increased Alcohol Seeking in Mice Lacking Gpr88 Involves Dysfunctional Mesocorticolimbic Networks. Biol Psychiatry. 84:202–212. [PubMed: 29580570]
9. Degiorgis L, Arefin TM, Ben-Hamida S, Noblet V, Antal C, Bienert T, et al. (2022): Translational Structural and Functional Signatures of Chronic Alcohol Effects in Mice. Biol Psychiatry. 91:1039–1050. [PubMed: 35654559]
10. Mandino F, Cerri DH, Garin CM, Straathof M, van Tilborg GAF, Chakravarty MM, et al. (2019): Animal Functional Magnetic Resonance Imaging: Trends and Path Toward Standardization. Front Neuroinform. 13:78. [PubMed: 32038217]
11. Heller EA, Cates HM, Pena CJ, Sun H, Shao N, Feng J, et al. (2014): Locus-specific epigenetic remodeling controls addiction- and depression-related behaviors. Nat Neurosci. 17:1720–1727. [PubMed: 25347353]

12. Hamilton PJ, Burek DJ, Lombroso SI, Neve RL, Robison AJ, Nestler EJ, et al. (2018): Cell-Type-Specific Epigenetic Editing at the Fosb Gene Controls Susceptibility to Social Defeat Stress. Neuropsychopharmacology. 43:272–284. [PubMed: 28462942]
13. Lorsch ZS, Loh YE, Purushothaman I, Walker DM, Parise EM, Salery M, et al. (2018): Estrogen receptor alpha drives pro-resilient transcription in mouse models of depression. Nat Commun. 9:1116. [PubMed: 29549264]
14. Nasseef MT, Ma W, Singh JP, Dozono N, Lancon K, Seguela P, et al. (2021): Chronic generalized pain disrupts whole brain functional connectivity in mice. Brain Imaging Behav. 15:2406–2416. [PubMed: 33428113]
15. Stafford JM, Jarrett BR, Miranda-Dominguez O, Mills BD, Cain N, Mihalas S, et al. (2014): Large-scale topology and the default mode network in the mouse connectome. Proc Natl Acad Sci U S A. 111:18745–18750. [PubMed: 25512496]
16. Robison AJ, Nestler EJ (2022): DeltaFOSB: A Potentially Druggable Master Orchestrator of Activity-Dependent Gene Expression. ACS Chem Neurosci. 13:296–307. [PubMed: 35020364]
17. Grueter BA, Robison AJ, Neve RL, Nestler EJ, Malenka RC (2013): ΔFosB differentially modulates nucleus accumbens direct and indirect pathway function. Proc Natl Acad Sci U S A. 110:1923–1928. [PubMed: 23319622]
18. Yim YY, Teague CD, Nestler EJ (2020): In vivo locus-specific editing of the neuroepigenome. Nat Rev Neurosci. 21:471–484. [PubMed: 32704051]
19. Goldstein RZ, Volkow ND (2011): Dysfunction of the prefrontal cortex in addiction: neuroimaging findings and clinical implications. Nat Rev Neurosci. 12:652–669. [PubMed: 22011681]
20. Friedman NP, Robbins TW (2022): The role of prefrontal cortex in cognitive control and executive function. Neuropsychopharmacology. 47:72–89. [PubMed: 34408280]
21. Mohan A, Roberto AJ, Mohan A, Lorenzo A, Jones K, Carney MJ, et al. (2016): The Significance of the Default Mode Network (DMN) in Neurological and Neuropsychiatric Disorders: A Review. Yale J Biol Med. 89:49–57. [PubMed: 27505016]
22. Xia Y, Driscoll JR, Wilbrecht L, Margolis EB, Fields HL, Hjelmstad GO (2011): Nucleus accumbens medium spiny neurons target non-dopaminergic neurons in the ventral tegmental area. J Neurosci. 31:7811–7816. [PubMed: 21613494]
23. Hikosaka O (2010): The habenula: from stress evasion to value-based decision-making. Nat Rev Neurosci. 11:503–513. [PubMed: 20559337]
24. Boulos LJ, Darcq E, Kieffer BL (2017): Translating the Habenula-From Rodents to Humans. Biol Psychiatry. 81:296–305. [PubMed: 27527822]
25. Hu H, Cui Y, Yang Y (2020): Circuits and functions of the lateral habenula in health and in disease. Nat Rev Neurosci. 21:277–295. [PubMed: 32269316]
26. Gardon O, Faget L, Chu Sin Chung P, Matifas A, Massotte D, Kieffer BL (2014): Expression of mu opioid receptor in dorsal diencephalic conduction system: new insights for the medial habenula. Neuroscience. 277:595–609. [PubMed: 25086313]
27. Boulos LJ, Ben Hamida S, Bailly J, Maitra M, Ehrlich AT, Gaveriaux-Ruff C, et al. (2020): Mu opioid receptors in the medial habenula contribute to naloxone aversion. Neuropsychopharmacology. 45:247–255. [PubMed: 31005059]
28. Bailly J, Allain F, Schwartz E, Tirel C, Dupuy C, Petit F, et al. (2022): Habenular Neurons Expressing Mu Opioid Receptors Promote Negative Affect in a Projection-Specific Manner. Biol Psychiatry.
29. Velasquez KM, Molfese DL, Salas R (2014): The role of the habenula in drug addiction. Front Hum Neurosci. 8:174. [PubMed: 24734015]
30. Lecca S, Meye FJ, Mameli M (2014): The lateral habenula in addiction and depression: an anatomical, synaptic and behavioral overview. Eur J Neurosci. 39:1170–1178. [PubMed: 24712996]
31. Yang Y, Wang H, Hu J, Hu H (2018): Lateral habenula in the pathophysiology of depression. Curr Opin Neurobiol. 48:90–96. [PubMed: 29175713]
32. Mathis V, Kenny PJ (2019): From controlled to compulsive drug-taking: The role of the habenula in addiction. Neurosci Biobehav Rev. 106:102–111. [PubMed: 29936111]

33. Aizawa H, Zhu M (2019): Toward an understanding of the habenula's various roles in human depression. Psychiatry Clin Neurosci. 73:607–612. [PubMed: 31131942]

34. Lee HW, Yang SH, Kim JY, Kim H (2019): The Role of the Medial Habenula Cholinergic System in Addiction and Emotion-Associated Behaviors. Front Psychiatry. 10:100. [PubMed: 30873055]

35. Golden SA, Heshmati M, Flanigan M, Christoffel DJ, Guise K, Pfau ML, et al. (2016): Basal forebrain projections to the lateral habenula modulate aggression reward. Nature. 534:688–692. [PubMed: 27357796]

36. Fanselow MS, Gale GD (2003): The amygdala, fear, and memory. Ann N Y Acad Sci. 985:125–134. [PubMed: 12724154]

37. Zhang WH, Zhang JY, Holmes A, Pan BX (2021): Amygdala Circuit Substrates for Stress Adaptation and Adversity. Biol Psychiatry. 89:847–856. [PubMed: 33691931]

38. Hu P, Lu Y, Pan BX, Zhang WH (2022): New Insights into the Pivotal Role of the Amygdala in Inflammation-Related Depression and Anxiety Disorder. Int J Mol Sci. 23.

39. Vialou V, Robison AJ, Laplant QC, Covington HE 3rd, Dietz DM, Ohnishi YN, et al. (2010): DeltaFosB in brain reward circuits mediates resilience to stress and antidepressant responses. Nat Neurosci. 13:745–752. [PubMed: 20473292]

40. Towers EB, Williams IL, Qillawala EI, Rissman EF, Lynch WJ (2023): Sex/Gender Differences in the Time-Course for the Development of Substance Use Disorder: A Focus on the Telescoping Effect. Pharmacol Rev. 75:217–249. [PubMed: 36781217]

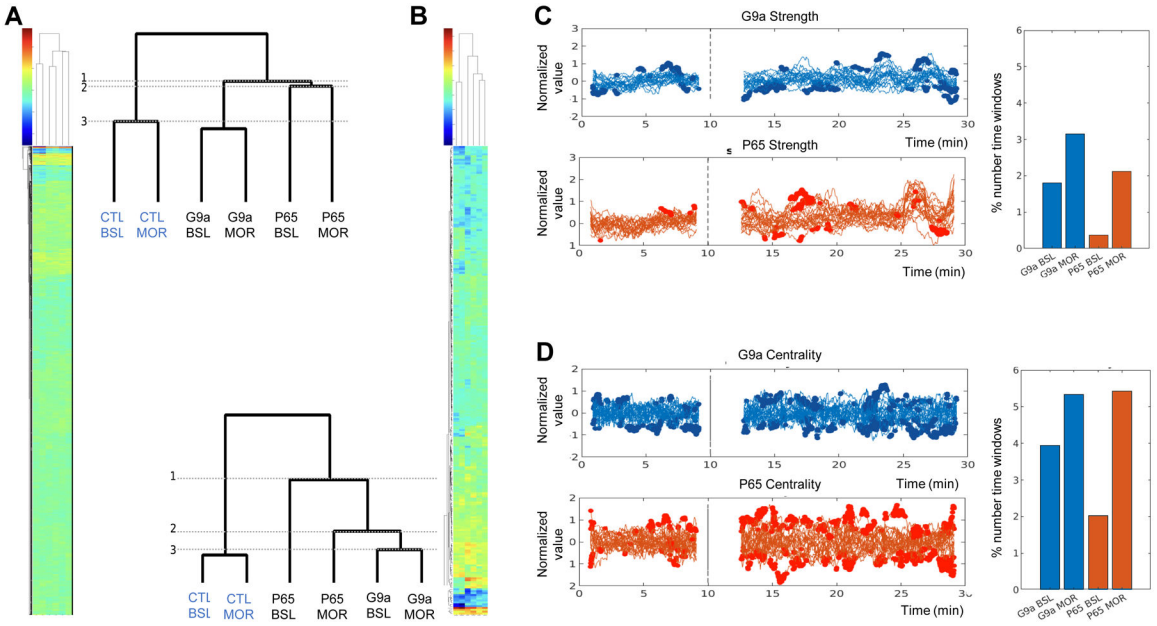

Figure 1. G9a and P65 mice differ from controls and differ from each other.

A, B. Stationary analysis is shown using CC values of 6 datasets (control values at baseline, CTL-BSL, or under morphine, CTL-MOR; G9a values at baseline, G9a-BSL, or under morphine, G9a-MOR; P65 values at baseline, P65-BSL, or under morphine, P65-MOR). **A.** Hierarchical clustering for 7140 functional connections between 120 seeds covering the entire brain, with an enlarged view of the dendrogram tree (up right). **B.** Hierarchical clustering for 253 functional connections between 23 selected seeds, with an enlarged view of the dendrogram tree (bottom left). 1, 2 and 3 shows subdivisions from larger to smaller clusters. **C, D.** Analysis of dynamic FC patterns. A sliding window approach was used to assess FC modifications along image acquisition (915 time windows in total, see Suppl Info), and shows the mean temporal evolution of strength (**C**) and centrality (**D**) for each group. For each time window, the value of strength or centrality is represented at the middle timepoint of the time window. Left panels: mean values for the 23 seeds are superimposed and bold indicates time windows where a significant difference is found between G9a or P65 and CTL values (t-test, $p<0.05$). X-axis, acquisition time in min; Y-axis, strength values normalized to their baseline values for each seed. Right panels: quantification. Percent number of time windows where G9a or P65 values significantly differ from CTL over total number time windows, and averaged over the 23 seeds. Values are shown for strength (**C**) and centrality (**D**) for each G9a and P65 group either under baseline (G9s-BSL, P65-BSL) or under morphine (G9a-MOR, P65-MOR). The % number of time windows where strength or centrality are different from controls, calculated for each ROI, are detailed in (Suppl Table S3).

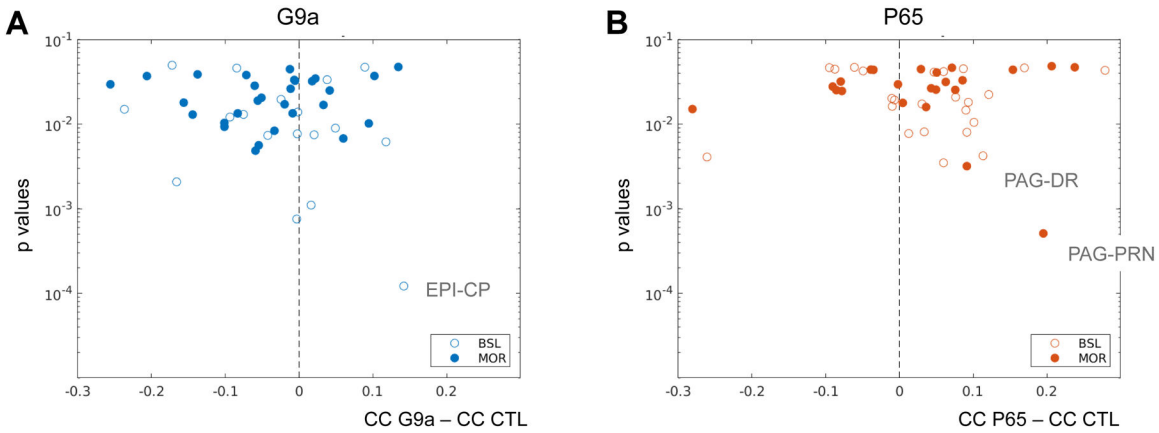

Figure 2. Functional connectivity is differently modified in G9a and P65 mice.

The graphs display seed pairs from G9a **(A)** and P65 **(B)** mice showing significantly different CC values from CTL animals, either during baseline (BSL, 1–9 min, open circles) or after morphine injection (MOR, 18–26 min, closed circles). Seed pairs are placed on the graph based on the direction of connectivity change vs CTL (X-axis, subtraction of absolute CC values between G9a and CTL groups in **A**, and between P65 and CTL groups in **B**, negative values for reduced FC and positive values for increased FC) and the statistical significance of the change (Y-axis, p values). **A.** In G9a mice, a larger number of seed pairs show reduced connectivity, and increased FC of the EPI-CP pair is most significant (BSL). **B.** In P65 mice, a larger number of connections show increased connectivity, and increased FC of PAG/PRN and PAG/DR pairs are most significant. All p values are reported in Suppl Table S4.

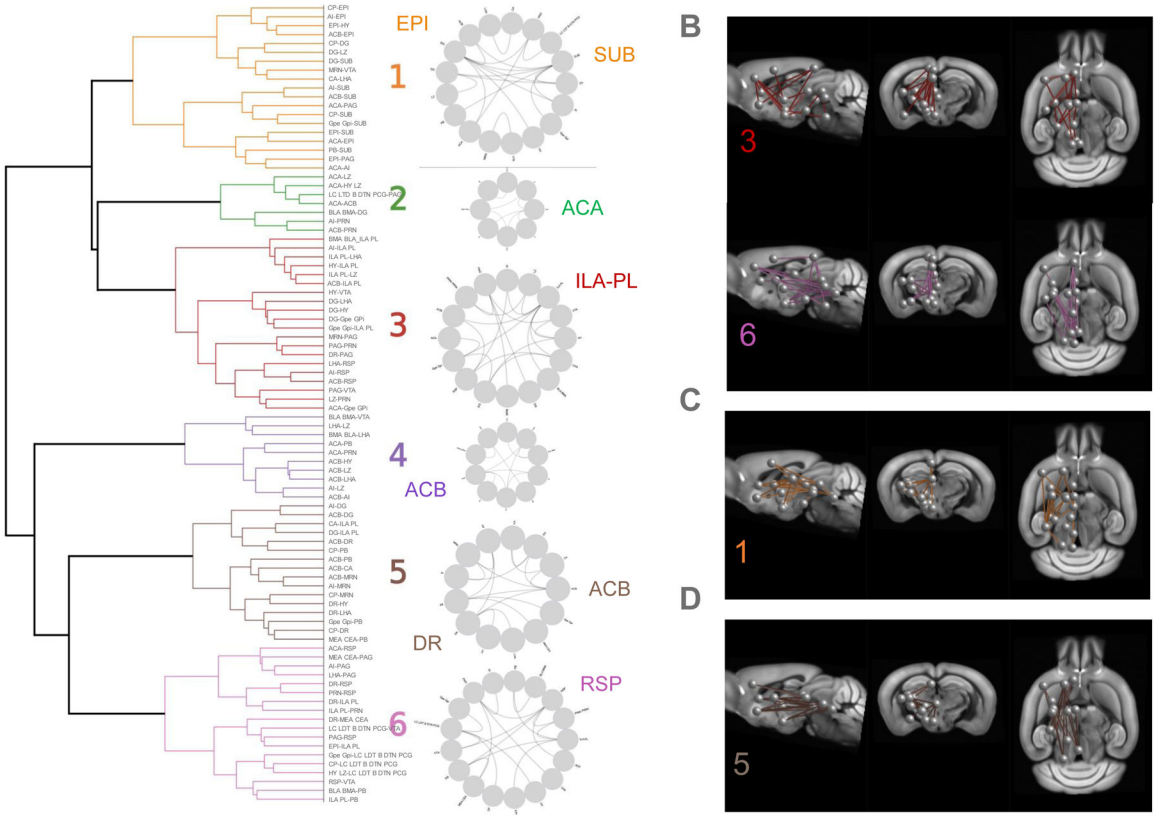

Figure 3. Network signatures of G9a and P65 effects on brain communication.

A. Left. Clustering of CC values from 90 significant seed pairs (Suppl. Table S4) across all individual animals of the study generated a dendrogram, with 6 major clusters. Right. Circular plots show seed pair connectivity within each cluster, and the most connected seed(s) are highlighted for each cluster. **B-D.** Visualization of networks showing connectivity modifications from CTL values from the box plot analysis (Suppl Fig S7), projected on the Allen Brain Atlas. **B.** Networks that are common to G9a and P65 treatment effects (clusters 3 and 6). **C.** Cluster 1 is different from CTL for the G9a treatment only. **D.** Cluster 5 is different from CTL for the P65 treatment only.

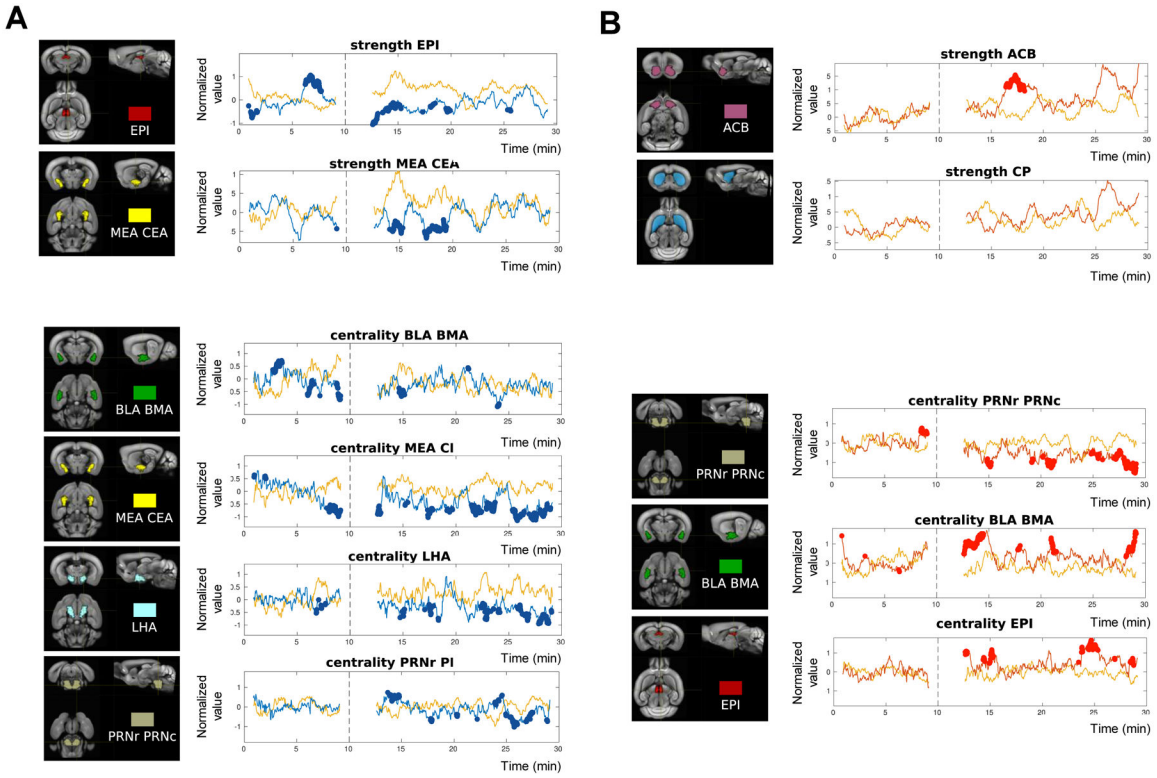

Figure 4. Analysis of dynamic FC patterns: remarkable modifications in G9a and P65 mice.

A sliding window approach was used to assess FC modifications along image acquisition (see Methods). Traces of strength and centrality are shown for individual seeds (see all traces superimposed in Fig. 1B). Seeds have been selected as they show the highest % number of time windows where strength (top) and centrality (bottom) are different from controls (see Suppl Table S3). The acquisition lasted 30 min in total with the last 20 min under morphine (10 mg/kg s.c.), and the time of injection is indicated as a dashed line. For each time window, the value of strength or centrality is represented at the middle timepoint of the time window. Time windows showing a significant difference with CTL strength or centrality are show in bold. **A.** G9a mice. Left. 3D-representaion of the seed. Right. Strongest modifications of strength (top) were observed for EPI and MEA-CEA, and of centrality (bottom) for BLA-BMA, MEA-CEA, LHA and PRN. **B.** P65 mice. Left. 3D-representaion of the seed. Right. Strongest modifications of strength (top) were observed for ACB, but the time difference was <15%. Strength of the nearby region CP was not modified. Centrality was most changed for PRN, BLA-BMA and EPI, and was observed mainly after the morphine challenge (bottom).